Research Article

Observation Frequency Analysis for Multiconstellation Radar Systems over the Mediterranean Sea

Marco D'Errico [1] **and Maria Daniela Graziano** [2]

[1]*Department of Engineering, Università degli Studi della Campania "Luigi Vanvitelli", Aversa 81031, Italy*
[2]*Department of Industrial Engineering, Università degli Studi di Napoli Federico II, Napoli 80125, Italy*

Correspondence should be addressed to Marco D'Errico; marco.derrico@unicampania.it

Observation frequency is analyzed over four areas of the Mediterranean basis where poaching, illegal fishing, and illegal trafficking of goods and people are active. To this end, a geometrical observation and dynamical model is utilized which accounts for multiple satellites and multiple orbital planes and is applied to SIASGE and Sentinel-1 missions. Statistics show that a few hours are needed in the mean to reobserve the same area.

1. Introduction

Surveillance of the Mediterranean basin is critical from humanitarian, environmental, and security points of view. Since maritime surveillance involves wide regions and very frequent observations of given areas, monitoring from space offers better operational performance with respect to aerial and maritime assets. As for surveillance of ships, the need to observe nonstationary small targets over a nonstationary background is an additional challenge. Synthetic aperture radar (SAR) has been identified as the key technology to fulfil application needs in the field of fisheries control, pollution control, and maritime border security [1].

SAR potential for ship detection has been analyzed for almost twenty years. Vachon [2] utilized RADARSAT-1 and Envisat data to show that length of detectable ship decreases at higher incidence angles thanks to the decrease of clutter level. Other analyses were proposed in [3] with application to fishery vessel monitoring and in [4] with major emphasis on the accuracy of detection obtained by alternating polarization data. Finally, Crisp [5] extensively analyses utilization of SAR imagery for ship detection. The ship wake has also been used for ship route identification in SAR images and a number of different techniques have been developed for wake detection [6–9] and to estimate ship velocity [8, 9].

On the one hand, spaceborne radar offers unique capabilities; on the other hand, a very strong limitation stands: a single satellite offers poor capability of reobservation of the same area on Earth. Nonetheless, SAR potential could be routinely utilized to implement a ship monitoring infrastructure based on the large number of currently flying and planned SAR missions. It is worth noting that spaceborne SAR evolution has led to the implementation of constellations with well-assessed radar and satellite design:

(i) Italian COSMO-SkyMed (CSK) [10] (4 satellites) and its follow-on COSMO second generation (CSG) [11] (2 satellites)

(ii) German military constellation SAR-Lupe [12] (5 satellites) and its follow-on SARah (3 satellites)

(iii) Canadian Radarsat Constellation [13] (3 satellites)

(iv) European Sentinel-1 mission [14] (2 satellites)

(v) Argentinian SAOCOM mission [15] (2 satellites)

(vi) Chinese Gaofen-3 [16] (3 satellites), Ludi-Tance (2 satellites), Gaofen-12 (3 satellites), and military Jianbing-5 and Jianbing-7 constellations

In addition, highly innovative constellations are under development and deployment. Finnish ICEYE [17] and American Capella [18] make use of very compact and lightweight design for both the bus and the payload. Further data can be found in [19, 20].

The innovation proposed and analyzed in the paper is the synergic use of multiple space assets to improve the observation frequency to the advantage of time-varying phenomena monitoring. From a model point of view, rather than simulating the orbits of multiple satellites, a cinematic/geometrical model is extended: it foresees satellite passes at any latitude. Such model was previously developed for a single radar satellite [21] and then extended to a multiple satellite configuration in the same orbital plane [22]. Finally, it has been extended in this paper, including the possibility to simulate multiplane constellations with different orbital parameters. We present its application to the Mediterranean Sea under the assumption of the availability of CSK, CSG, Sentinel-1, and SAOCOM constellations. Being either part of the Copernicus asset or of the SIASGE system (CSK, CSG, and SAOCOM), their synergic use is a pursuable goal.

The paper is organized as follows: Section 2 analyses the area to be observed and its schematization in a discrete set of targets, while Section 3 identifies initial conditions of the selected constellations and their relative phasing. Then, Section 4 shows the statics of reobservations time attained on such area.

2. Target Areas and Schematization

"In 2018, our sea suffered a real frontal attack, with 20,437 ascertained infringements, 20% more than the previous year and, even, 28.5% more than in 2016". This is how Legambiente in the 2019 annual report launches its alarm on the state of the Italian waters and coasts and on failings of current prevention and control systems. These numbers testify the need for further intervention actions [23]. At a national level, the coasts of the major islands are the scenarios in which illegal fishing is widespread: Sicily holds the sad record, with almost a thousand ascertained infringements. Sardinia, on the other hand, has the record for fish products seized with 129,000 kg in one year. Bluefin tuna, mollusks, sea urchins, and other fishes are caught breaking the rules that protect the species and regulate fishing seasons. Internationally, it has been estimated that illegal fishing represents 19% of the total catch with an economic value of 10 billion euros each year [24]. There are 29 Italian marine protected areas and 2 underwater parks, which protect a total of 228,000 hectares of sea and 700 kilometers of coastline [25]. The possibilities for on-site monitoring of such large areas are therefore very limited. A World Wide Fund for Nature (WWF) survey has highlighted how waste, plastics at sea, tourism, and maritime traffic pose an increasing pressure on the survival of biodiversity in Italian marine protected areas. However, it is poaching and illegal fishing that are the main and most widespread problems. The analysis also showed that, with reference to large marine protected areas (> 10000 hectares), the illegal fishing is prevalent.

In addition, illegal trafficking of goods and people has a transnational competence. In the Mediterranean Sea, the most used routes are from Libya, Tunisia, and Turkey to Italy and from Morocco to Spain, with almost daily tragic reports. Less known is the illegal maritime trade in goods (drugs and weapons, mainly). Italy is one of the main import routes in Europe given its geographical position in the center of the Mediterranean and the extension of its coastal areas. In its report on Italian port security 2018, the Italian port security assessed that the most complex challenge for national surveillance systems is cocaine traffic on medium-long distances [26]. The European border control agency Frontex has identified two specific areas where satellite monitoring can help fight the illegal trafficking of goods towards the European coasts: the Alboran Sea, between Gibraltar and Melilla, and the Adriatic Sea between the Albanian and Italian coasts [27].

Therefore, four areas are identified to investigate potential frequency of observation of systems of constellations with potential applications in the fields of illegal fishing, illegal trafficking control, and protected marine areas monitoring (Figure 1, Table 1). They correspond to quadrangular areas in latitude/longitude.

Since the observation frequency analysis algorithm relies on discrete modelling of the Earth, to have a consistent representation of the different areas, they must be sampled with identical linear spacing. Therefore, each area must be adequately sampled considering its extensions in both latitude and longitude and considering that a constant linear spacing implies that the number of sample points must decrease with longitude to account for the reduction of local parallel length. The selected areas have been sampled assuming to represent the equator with 3000 points, which corresponds to a linear spacing of about 13.4 km. Therefore, each meridian is sampled with such spacing as well as each parallel (Figure 2). We verified with a simulation on the whole globe that a further increase of the number of points does not modify reobservation time statistics significantly. Finally, each area has been sampled with a different number of sample points (Table 1) to be equivalently represented by a statistical point of view.

3. Constellation Initial Conditions

Considering the number of radar constellations which have been deployed or are under development, we select the following assets to analyze the frequency of observation:

(i) Italian COSMO/SkyMed (CSK) and Cosmo second generation (CSG)

(ii) Argentinian SAOCOM 1

(iii) European Sentinel-1

CSK and CSG are already operated as a single system. In addition, SAOCOM 1 was developed by Argentina under coordination with Italy. Furthermore, CSK and CSG are national assets of Copernicus, which include Sentinel-1. Therefore, agreements are already in place to coordinate
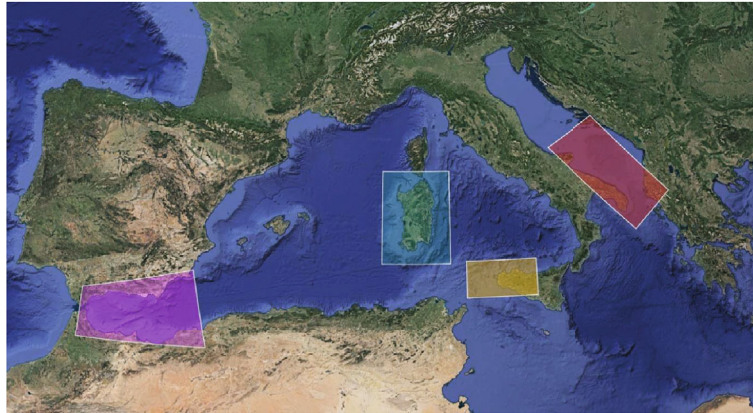
Figure 1: Selected areas of interest. From left to right: Strait of Gibraltar, Sardinia, West Sicily, and Southern Adriatic Sea.

Table 1: Areas of interest coordinates.

Area of interest	Center latitude (°)	Center longitude (°)	No. of points
(1) Adriatic Sea	41.218	17.860	554
(2) Sardinia	39.987	8.9978	547
(3) West Sicily	37.894	12.663	253
(4) Alboran Sea	36.152	-2.9597	742

satellite operations and to exchange mission data. Selected constellations consist of 4 satellites (CSK) and 2 satellites (CSG) sharing the same orbital plane and with coordinated phasing between satellites, 2 satellites with orbital planes close to those of CSK and CGS (SAOCOM 1), and 2 satellites sharing another orbital plane (Sentinel-1). We then have 10 satellites available: 2 in C-band (Sentinel-1), 2 in L-band (SAOCOM 1), and 6 in X-band.

To perform repetitivity analysis effectively, it is necessary to identify the relative geometries of the different orbits and the in-plane phasing among the satellites of the same constellation and of different constellations. This assessment has been performed by available data in literature [28–35] and by analyzing two-line element (TLE) sets of all satellites to assess unknown parameters and for an overall geometry verification.

Table 2 lists all data derived from the literature. They are not sufficient to describe satellite motion in time with respect to the rotating Earth, which is essential to derive target observation frequencies. Figure 3 shows the relative phasing of CSK/CSG constellation.

In order to simulate constellation motion with respect to the Earth, it is necessary to estimate ascending nodes' longitude and satellites' argument of latitude at the same epoch. Since such data are not available in the literature, they have been derived from TLE which were downloaded from satellite tracking websites (e.g. http://www.celestrak.com).

Unfortunately, TLE are not available at the same epoch for all satellites. Therefore, satellite orbital elements must be properly synchronized at a unique universal time to attain coherent initial conditions to propagate constellations.

The first step has been synchronization of all satellites at the time of the CSK-1 TLE data used as reference. In particular, right ascension of the ascending nodes and perigee anomalies have not been modified because the time difference is of the order of thousands of seconds, with the maximum Δt of about 3 hours for SAOCOM 1A: (a) precession of line-of-nodes is mainly related to J_2 perturbation, and it is at least three orders of magnitude smaller than the mean anomaly rates; (b) all orbits are frozen in eccentricity, thus perigees only oscillate very slowly around the anomaly of 90°. Instead, it is necessary to correct the mean anomaly, whose angular rates are of the order of 10^{-3} rad/s. Corrections have been made and arguments of latitude (satellite anomalies with respect to the ascending node) estimated at the same time considering the mean anomaly rate for each satellite.

CSK, CSG, and SAOCOM satellites' relative phasing at the time of CSK-1 TLE is shown in Figure 4, where it must be considered that the orbital planes of SAOCOM satellites are slightly different than those of CSK and CGS ones. In addition, it is worth considering that at the time of TLE download, CSG 2 was still maneuvering after launch to reach its nominal positions in the constellation (in fact, experimental perigee anomaly, eccentricity, and mean anomaly were incompatible with the nominal ones derived from literature).

TLE analysis clarifies the planar sequence of CSK, CGS, and SAOCOM. For SAOCOM, some discrepancies remain: (a) SAOCOM satellites seem separated by 166° anomaly shift instead of the nominal 180° value reported in the literature; (b) SAOCOM satellites are phased of about 45° and 30° with respect to COSMO instead of the nominal 32.5° reported in the literature (10 minutes). Since the observation frequency estimation process requires the longitudes of the ascending nodes, considering that the time of passage of CSK-1 on the ascending node is February 8th, 2022, at 4 h 28 m 43.76 s, Greenwich meridian right ascension was computed (205.45°). Therefore, we get Table 3.

Some assumptions are needed to resolve discrepancies between nominal parameters and experimental ones which can be affected by the particular situation caused by CSG-2 launch and operations. Thus, since CSG 2 satellite was maneuvering, its anomaly will be forced at its nominal value. Then, as for Sentinel-1 constellation, the ascending nodes
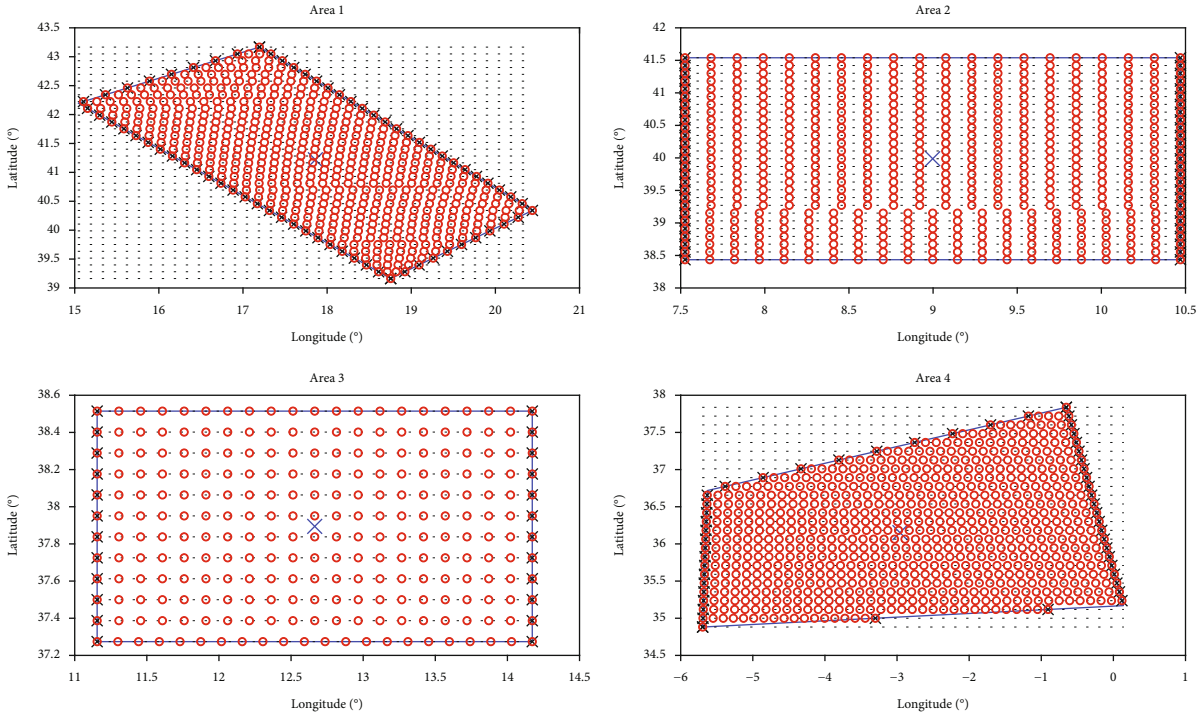
Figure 2: Discrete schematization of the four selected areas of interest.

Table 2: Orbit data as derived from literature.

	CSK, CSG	SAOCOM 1	Sentinel-1
Orbit	Sun-synchronous frozen	Sun-synchronous frozen	Sun-synchronous frozen
Ascending node local time	6 a.m.	6 a.m.	6 p.m.
Altitude (km)	619.6	619.6	693
Inclination (°)	97.86	97.86	98.18
Eccentricity	1.18×10^{-3}	N/A	N/A
Satellite phasing (°)	See Figure 3	180°	180°
Repetition cycle	237/16	237/16	175/12
Elevation angle range (°)	22.7-44.3	20-50 (incidence)	20-45 (incidence)

Figure 3: In-plane distribution of CSK and CGS satellites (reproduced from [28]).

FIGURE 4: In-plane distribution of CSK, CSG, and SAOCOM satellites as derived from TLE at the time of the TLE of CSK 1 satellite.
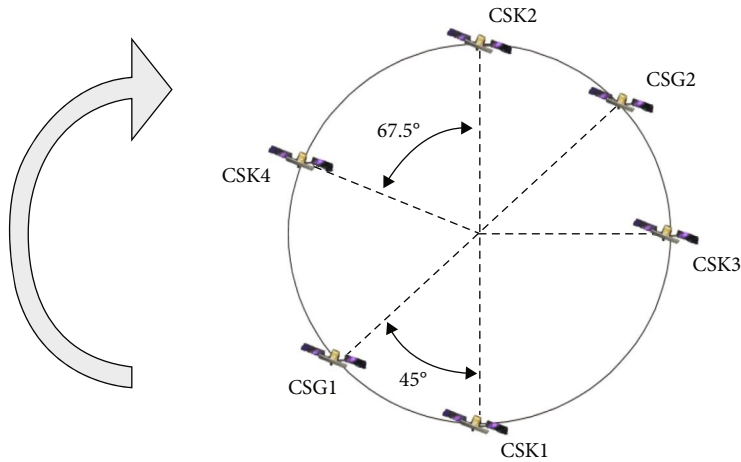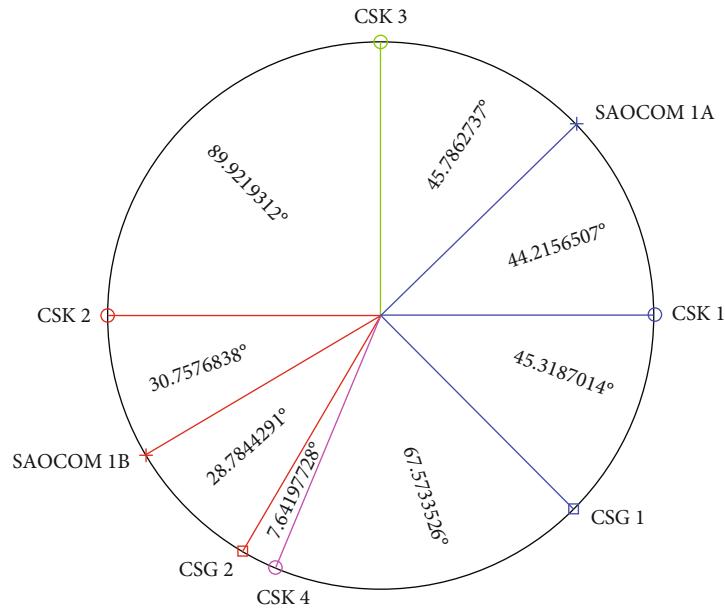
TABLE 3: Longitude of ascending nodes and satellite arguments of latitude (nodal anomaly) at UT: February 8th, 2022, at 4 h 28 m 43.76 s.

Satellite	Right ascension of the ascending node (°)	Longitude of the ascending node (°)	Satellite argument of latitude (°)
CSK 1			0
CSK 2			179.92
CSK 3			90.002
CSK 4	224.69	19.243	247.11
CSG 1			314.68
CSG 2			239.47
SAOCOM 1A	227.60	22.152	44.216
SAOCOM 1B	226.70	21.251	210.68
Sentinel-1A	48.588	-156.86	50.071
Sentinel-1B	48.380	-157.07	227.42

TABLE 4: Selected constellation geometry at UT: February 8th, 2022, at 4 h 28 m 43.76 s.

Satellite	Satellite argument of latitude (°)	Longitude of the ascending node (°)
CSK 1	0	
CSK 3	90	
CSG 2	135	
CSK 2	180	19.2435
CSK 4	247.5	
CSG 1	315	
SAOCOM 1A	32.5	
SAOCOM 1B	212.5	21.7018
Sentinel-1A	50.0709	
Sentinel-1B	230.0709	156.9665

differ by 0.2°, which is certainly an acceptable discrepancy with respect to what is expected from the literature. Their relative phasing is 177° instead of the 180° expected, but again, such difference seems acceptable considering real data analysis. Therefore, Sentinel-1A argument of latitude could be assumed from TLE and Sentinel-1B rephased at 180°. Ascending node longitude will be fixed at the mean value of the two data.

SAOCOM constellation poses major challenges of interpretation, probably due to a lack of nominal information derived from literature. Real data do not confirm satellite phasing from one another (166° instead of 180°) and from CSK (44° and 30° instead of 32.5°). As expected, they have a small (3°-4°) difference in ascending node right ascension which is probably related to satellite management and reduction of collision risk with CSK/CSG satellites. Therefore, to the aim of frequency of observation simulation, SAOCOM satellites are forced at their nominal phasing of 180°, and we relocate them at 32.5° from the closest CSK/
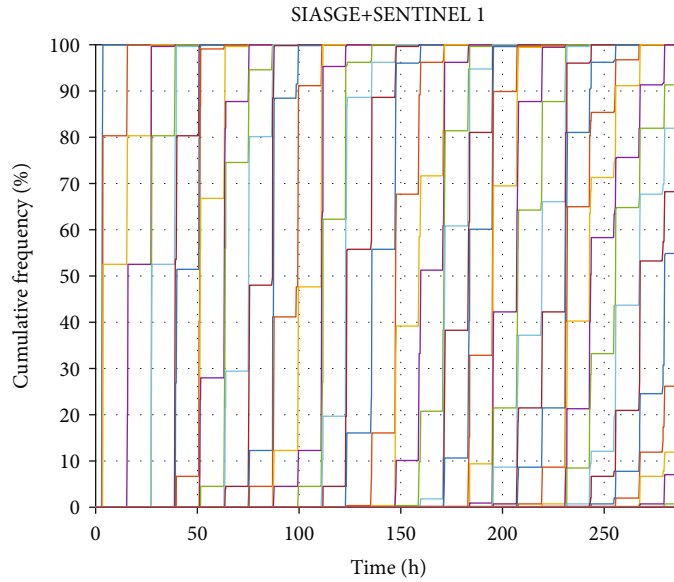
FIGURE 5: Cumulative frequency of the time of passage over the same target for area 1: Adriatic Sea.
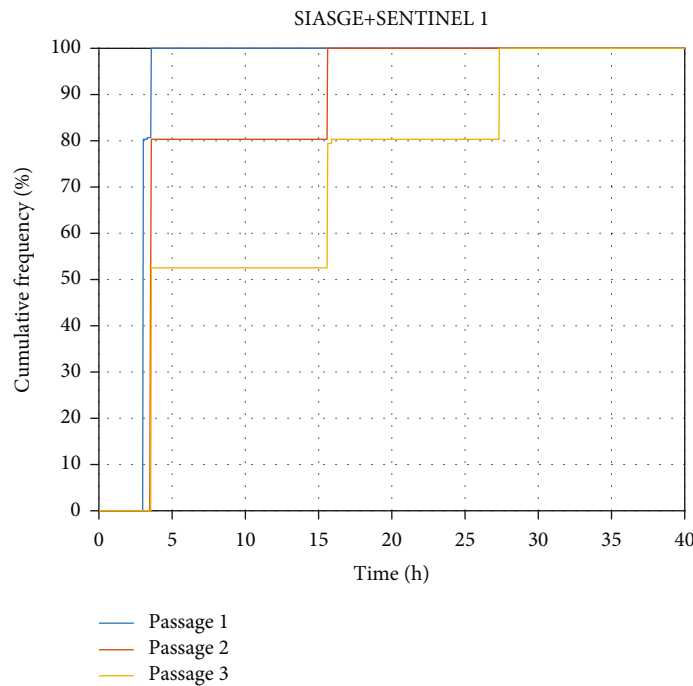
FIGURE 6: Cumulative frequency of the time of passages 1-3 over the same target for area 1: Adriatic Sea.

CSG satellite. Line-of-nodes are set equal averaging the two ascending node longitudes. Table 4 summarizes the set of initial conditions which have finally been assumed.

4. Statics of Observation Frequency

In-depth details on the original model and its extension to account for both left and right pointing and for whatsoever number of satellites with a selectable in-plane phase angle but in the same orbit plane can be found in [36]. Briefly summarizing, the analysis of repetitivity provides the time required to observe each selected target and relative statistics. Evaluation of observation capabilities is performed by dividing the repetition periods into time elements and determining when each target is in the sensor potential swath. To this end, first, the access area on a given parallel on the grounds of maximum and minimum sensor elevation angles is determined. The satellite motion is described considering the secular perturbations of a Keplerian circular orbit that cause the perigee and the ascending node precession. Then, the grid of ascending nadirs and associated times of passage are computed considering the angle between two adjacent
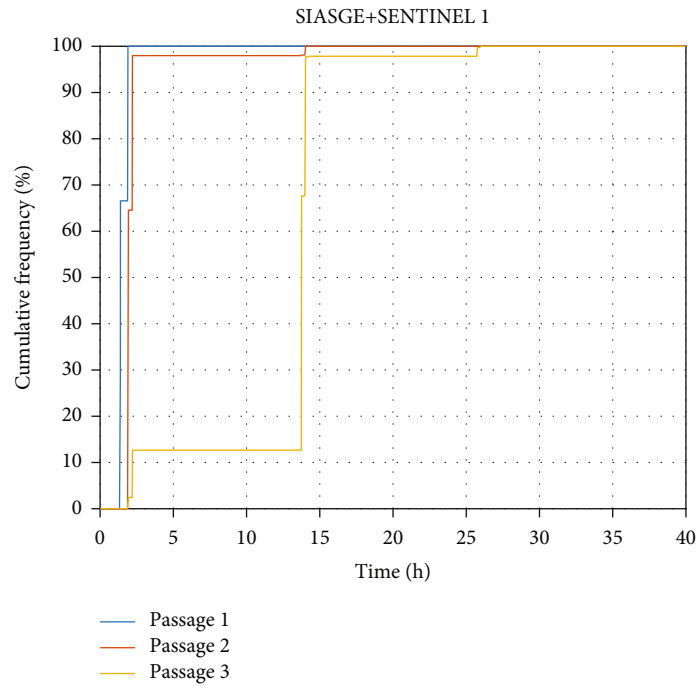
FIGURE 7: Cumulative frequency of the time of passages 1-3 over the same target for area 4: Strait of Gibraltar.
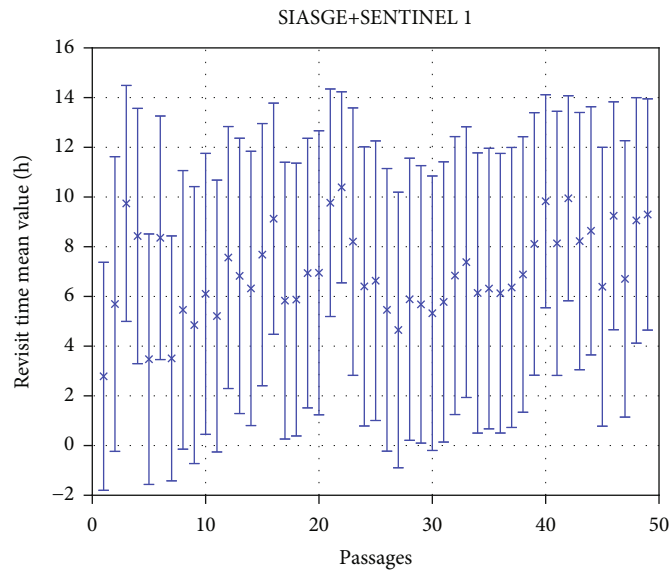
FIGURE 8: Revisit time mean value and std. deviation for area 1: Adriatic Sea.

ascending nodes and the angle between two successive ascending nodes as a function of the repetition factor. The angle between the nth ascending and descending nodes depends on the satellite motion and the Earth's rotation with respect to the nodal line (see the Appendix for details). The observation geometry of satellites is analyzed to compute the angle subtended by the arc between the two points on the parallel corresponding to the minimum and the maximum off-nadir angle. Thus, for any given node on the parallel, the parallel arc observed by a SAR can be determined [21] to verify if a given target can be observed. Finally, for each target, the times of the first, second, and n^{th} observations are determined in the repetition period as well as the elapsed time between observation i and $i + 1$. Relative observation frequency is derived as a function of time by dividing the number of targets under potential observation at the given time by the total number of targets. The cumulative frequency at a given time is the sum of relative frequency at previous times. Such statistics are derived for both observation time and time interval between successive observations.

The analysis is conducted over the four selected areas of interest providing the cumulative frequency of passages over
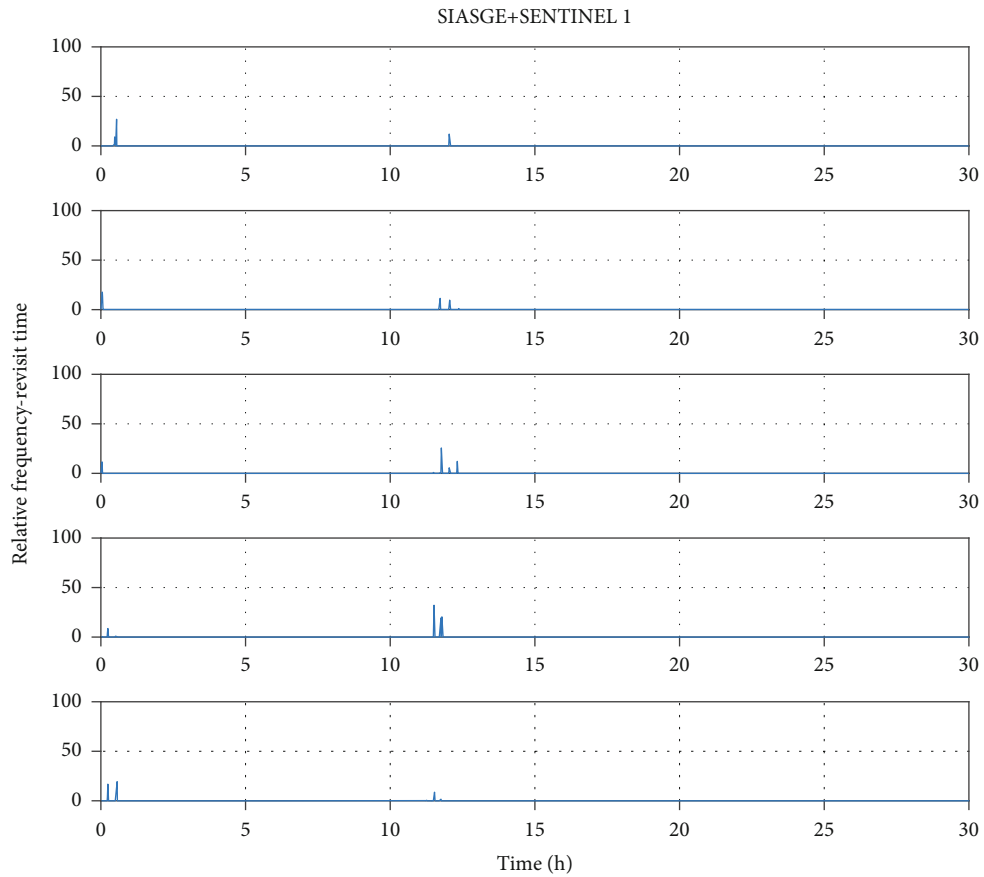
Figure 9: Revisit time relative frequency for area 1: Adriatic Sea.
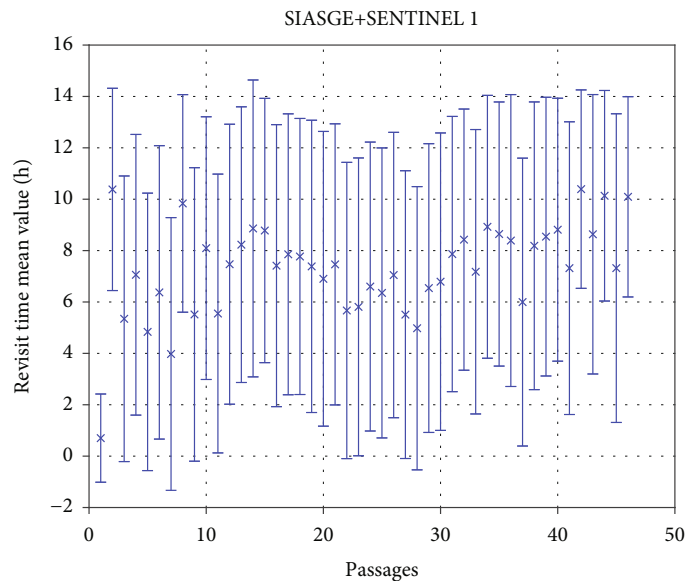
Figure 10: Revisit time mean value and std. deviation for area 4: Strait of Gibraltar.

the area of interest considering the three missions which integrate the SIASGE constellation and the ESA Sentinel-1 mission.

Let us first consider the area of interest 1 (Adriatic Sea). Figure 5 highlights the cumulative frequency of the time of passage over a given target for all the completed passages in the simulation time. Figure 6 highlights the first three passages: the first passage is completed in about 3.6 hours; the second passage is completed in about 15.6 hours; the third passage is completed in about 27.3 hours. In addition, we
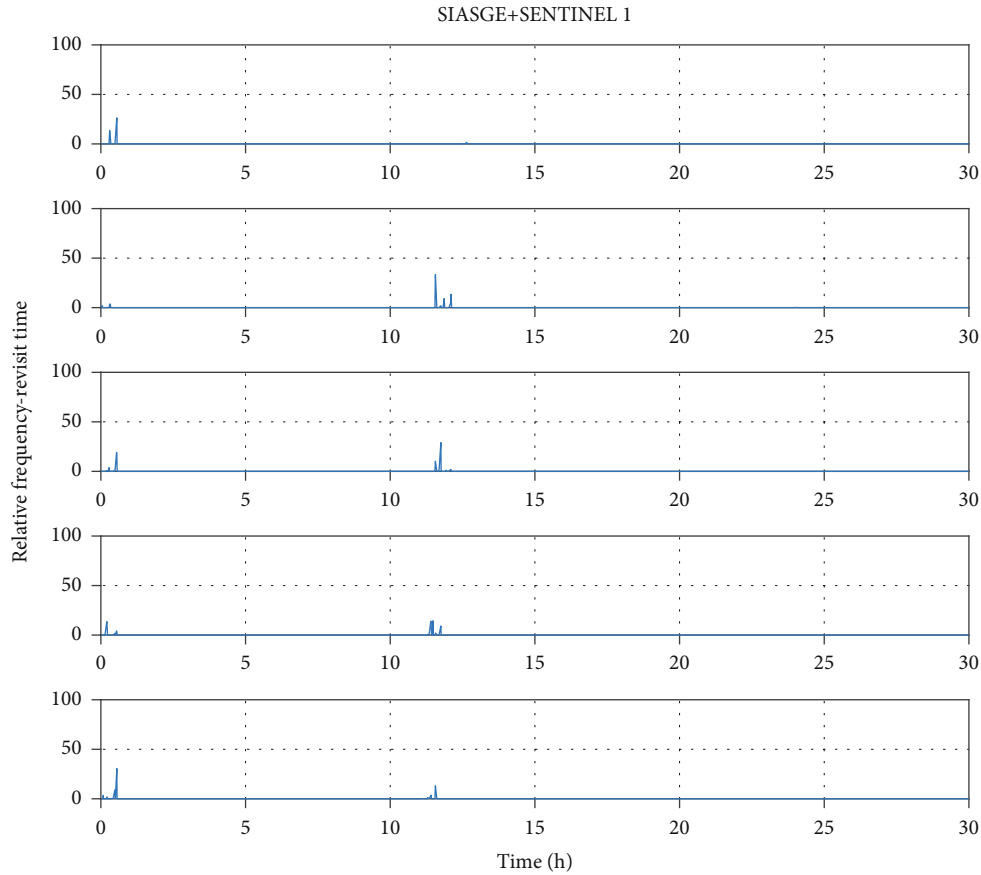
FIGURE 11: Revisit time relative frequency for area 4: Strait of Gibraltar.

TABLE 5: Statistics of revisit time.

Area	Mean (h)	Std. (h)	Mean (h) 95%	Std. (h) 95%	Mean (h) 90%	Std. (h) 90%
Adriatic Sea	6.95	5.29	12.2	0.383	12.0	0.283
Sardinia	7.04	5.13	12.0	1.70	11.5	2.34
West Sicily	7.07	5.06	12.0	0.357	11.9	0.347
Alboran Sea	7.30	5.31	12.0	1.74	11.8	1.71

can state that the 80% of the area can be observed: in about 3 hours for the first time; in about 3.6 hours for the second time; in about 15.9 hours for the third time. These results highlight that a good understanding of the observation capability is not only given by analyzing full coverage of the area of interest. Rather, it is necessary to have additional criteria describing how rapidly coverage grows in time.

As for the largest area of interest (area 4, Strait of Gibraltar), Figure 7 shows that the first and second passages are completed quickly, reaching almost 100% in less than three hours. On the other hand, the third passage rises very slowly, and almost 15 hours is required to exceed 95% coverage.

To gain a better understanding of repetitive performance, the mean values and the standard deviations of revisit time are evaluated considering all completed passages. For the Adriatic Sea (area 1), 49 passages are completed (Figure 8), and the revisit time mean value is about 6.95 h with a standard deviation of 5.29 h. In addition, due to large value of such standard deviation, mean values and standard deviations of time intervals required to reobserved 90% and 95% of the targets are also computed. The mean value (standard deviations) of time required to reobserve 95% of targets is 12.2 hours (23 minutes). Analysis at 90% target reobservation shows a great reduction of standard deviation: mean value of 12.0 hours with a standard deviation of about 17 minutes. Revisit time relative frequencies have been plotted in Figure 9 for the first five passages. First, it is worth noting that observations occur within a time span of a few hours thanks to multiple constellations, but successive observations happen in about 12 h since all constellations have close lines-of-nodes.

This analysis has been performed over all areas. Figures 10 and 11 show revisit time statistics for the Strait of Gibraltar which are characterized by the same behavior. All results are synthesized in Table 5 to show that performances are similar among different areas. The mean time

FIGURE 12: Geometry to define locations of ascending and descending passes over a parallel at a given latitude.

to revisit the area is always around 6 hours with a standard deviation of about 5 hours. The mean time to revisit the 95% of the targets is again almost equivalent, as well as for 90% of the target and in both cases of the order of 12 hours. In these latter cases, standard deviations increase from few tens of minutes to almost two hours for Sardinia and Gibraltar. This behavior could be related to Area extension and shape. Gibraltar and Sardinia are wide areas (742 and 554 points, respectively), while Sicily is the smallest (253 points). Adriatic Sea is also a wide area but, differently from Gibraltar and Sardinia which are close to rectangles in longitude and latitude, it is shaped almost along the quasipolar satellites' tracks, which probably reduces the standard deviation. In addition, performances are similar because all areas of interest are close in both latitude and longitude.

5. Conclusions

This paper approached the problem of evaluating reobservation capabilities of complex satellite systems based on synergic use of different radar constellations. The study has been focused on a system which makes use of COSMO-SkyMed, Cosmo second generation, SAOCOM 1, and Sentinel-1 which totalize ten SAR satellites belonging either to Copernicus or (and) to SIASGE. Operational coordination and data exchange policy have already been agreed for such systems. The investigated region is the Mediterranean basin and, in particular, four areas where poaching, illegal fishing, and illegal trafficking of goods and people are common activities. Current control systems have shown their weakness and would benefit from effective space observatories.

From a mathematical point of view, an existing geometrical observation and dynamical model are extended to multiplane satellite systems. It requires that areas under

observation are adequately sampled in sets of discrete targets. In addition, all satellite orbital parameters must be synchronized at a unique epoch. The authors have shown how to adequately sample the target areas and a method to fix satellite data working on both literature and two-line element data set to derive unknown parameters and resolve ambiguities.

The analysis of observation frequency has shown that performance is similar over the Mediterranean basin with slight differences depending on the extension and shape of selected areas. In addition, it has been shown that reobservations occur in rapid sequence at a fraction of the orbital period with "blind" time interval of about 12 h in average. Therefore, the use of multiple satellite systems is extremely beneficial because it allows for a dense sequence of successive observations by different satellites, which is a great advantage with respect to a single satellite and a single constellation. Nonetheless, it still fails to ensure continuity of observation throughout the day.

This limitation is not related to the selected constellations because all radar constellations share similar line-of-nodes, with the ascending local time set at dawn or at sunset. Such limitation would take great advantage from the development of innovative approaches in spaceborne SAR (such as ICEYE and Capella), which foresee different orbital planes and ascending node local times.

Appendix

The satellite motion is described considering the J_2 secular perturbations of a Keplerian orbit [37], consisting of perigee ($\dot{\omega}$) and the ascending node ($\dot{\Omega}$) precessions and a modification of the mean motion ($\dot{M}$). The repetition factor (Q) is defined for a repetitive orbit as the integer number of

satellite revolutions (R) divided by the integer number of Earth rotations (N) with respect to the ascending node [38].

$$Q = \frac{R}{N} = \frac{\dot{M} + \dot{\omega}}{\Omega_{\oplus} - \dot{\Omega}}, \tag{A.1}$$

where $\Omega_{\oplus}$ is the Earth's rotation rate. Extending the wording of the ascending and descending nodes from the equatorial plane to any parallel at any latitude ϕ, two adjacent (in space) ascending nodes are spaced by an angle $2\pi/R$, whereas two successive (in time) ascending nodes are spaced by $2\pi/Q$. The same stands for descending nodes [39]. Thus, angular spacing between the first and the nth ascending node and elapsed time are given by:

$$A_1\widehat{O}A_n = (n-1)\frac{2\pi}{Q}, \tag{A.2}$$

$$\Delta t_{A_1 A_n} = (n-1)\tau, \tag{A.3}$$

where τ is the nodal period.

The angular spacing between the nth ascending (A_n) and descending (D_n) nodes is computed in Figure 12 and depends on a geometrical contribution plus the Earth's rotation in the time required by the satellite to fly from A_n to D_n.

$$A_n\widehat{O}D_n = 2\cos^{-1}\left(-\frac{\tan\phi}{\tan i}\right) + \frac{2\pi}{Q}\begin{cases} f & \text{if } \phi \geq 0, \\ 1-f & \text{if } \phi \leq 0, \end{cases}$$
$$f = \frac{1}{\pi}\sin^{-1}\left\{\cos\phi\sin\left[\cos^{-1}\left(-\frac{\tan\phi}{\tan i}\right)\right]\right\}. \tag{A.4}$$

The corresponding time interval is as follows:

$$\Delta t_{A_n D_n} = \tau\begin{cases} f & \text{if } \phi \geq 0, \\ 1-f & \text{if } \phi \leq 0. \end{cases} \tag{A.5}$$

It is worth underlying that Equations (A.2)–(A.5) extend to any latitude in the model by King [40], which only stands for the equator.

In addition, in Figure 12, the angular spacing between the 1st ascending node on the equator ($A_{1,E}$) and the 1st ascending node on the parallel at latitude ϕ (A_1) can also be computed. Again, it is the sum of a geometrical contribution plus the Earth's rotation in the time required by the satellite to fly from $A_{1,E}$ to A_1.

$$A_{1,E}\widehat{O}A_1 = \sin^{-1}\left(-\frac{\tan\phi}{\tan i}\right) + \frac{1}{Q}\sin^{-1}\left(\frac{\sin\phi}{\sin i}\right),$$
$$\Delta t_{A_{1,E} A_1} = \frac{1}{2\pi}\sin^{-1}\left(\frac{\sin\phi}{\sin i}\right)\tau. \tag{A.6}$$

Therefore, given the ascending node's right ascension and the associated time of the passage on the ascending node of a single satellite, the times and longitudes of every ascending/descending passage can be derived by implementing the above equations. For a constellation of satellites sharing the same orbital plane, satellite in-plane relative phasing suffices to simulate the whole constellation. In the case of either constellations with multiple orbital planes or constellations of constellations, the model requires to identify the location of the first satellite of each orbital plane at a single universal time.

Data Availability

Utilized data are cited in paper's references which also describe utilized algorithms.

Conflicts of Interest

The authors declare that they have no conflicts of interest.

Acknowledgments

References

[1] H. Greidanus, "Satellite imaging for maritime surveillance of the European seas," in *Remote Sensing of the European Seas*, V. Barale and M. Gade, Eds., pp. 343–358, Springer, New York, NY, USA, 2008.

[2] P. W. Vachon, "Ship detection in synthetic aperture radar imagery," in *Proceedings of OceanSAR*, pp. 1–10, St. John's, Canada, 2006.

[3] G. Lemoine, J. Chesworth, G. Schwartz-Juste, N. Kourti, and I. Shepherd, "Near real time vessel detection using spaceborne SAR imagery in support of fisheries monitoring and control operations," *Proceedings of IGARSS*, vol. 7, pp. 4825–4828, 2004.

[4] X. Li and J. Chong, "Processing of Envisat alternating polarization data for vessel detection," *Geoscience and Remote Sensing Letters*, vol. 5, no. 2, pp. 271–275, 2008.

[5] D. J. Crisp, *The State-of-the-Art in Ship Detection in Synthetic Aperture Radar Imagery*, Australian Government Department of Defence, 2004, doc# DSTO–RR–0272.

[6] M. T. Rey, J. Tunaley, J. T. Folinsbee, P. A. Jahans, J. A. Dixon, and M. R. Vant, "Application of radon transform techniques to wake detection in Seasat-A SAR images," *IEEE Transactions on Geoscience and Remote Sensing*, vol. 28, no. 4, pp. 553–560, 1990.

[7] A. C. Copeland, G. Ravichandran, and M. M. Trivedi, "Localized radon transform-based detection of ship wakes in SAR images," *IEEE Transactions on Geoscience and Remote Sensing*, vol. 33, no. 1, pp. 35–45, 1995.

[8] G. Zilman, A. Zapolski, and M. Marom, "The speed and beam of a ship from its wake's SAR images," *IEEE Transactions on Geoscience and Remote Sensing*, vol. 42, no. 10, pp. 2335–2343, 2004.

[9] M. D. Graziano, M. D'Errico, and G. Rufino, "Wake component detection in X-band SAR images for ship heading and velocity estimation," *Remote Sensing*, vol. 8, no. 6, p. 498, 2016.

[10] F. Covello, M. L. Battagliere, and A. Coletta, "Overview and exploitation of the fully deployed COSMO-SkyMed constellation," in *Proceedings of the 63rd International Astronautical Congress*, pp. 1–5, Naples, Italy, 2012.

[11] D. Calabrese, F. Carnevale, V. Mastroddi et al., "CSG system performance and mission," in *Proceedings of the 11th European Conference on Synthetic Aperture Radar*, pp. 1–4, Hamburg, Germany, 2016.

[12] D. Koebel, C. Tobehn, and B. Penné, "OHB platforms for constellation satellites," in *Proceedings of the 5th IAA Symposium on Small Satellites for Earth Observation*, pp. 1–8, Berlin, Germany, 2005.

[13] A. A. Thompson, "Innovative capabilities of the RADARSAT constellation mission," in *Proceedings of the 8th European Conference on Synthetic Aperture Radar*, pp. 1–3, Aachen, Germany, 2010.

[14] D. T. Geudtner, P. Snoeij, A. Ostergaard, I. Navas-Traver, B. Rommen, and M. Brown, "Sentinel-1 system overview and performance," in *Proceedings of the ESA Living Planet Symposium*, p. 96, Edinburgh, UK, 2013.

[15] L. Frulla, J. Medina, J. Milovich, G. R. Ortega, and M. Thibeault, "SAOCom misson overview," in *Proceedings of CEOS SAR Calibration and Validation Workshop*, pp. 1–15, Fairbanks, AK, USA, 2011.

[16] Q. Wei, Y. Shao, and X. Wang, "Preliminary evaluation of Gaofen-3 quad-polarized SAR imagery for Longbao protected plateau wetland reserve," *Journal of Sensors*, vol. 2019, Article ID 8789473, 7 pages, 2019.

[17] V. Ignatenko, O. Dogan, D. Muff et al., "ICEYE microsatellite SAR constellation status update: spotlight extended area mode, daily coherent ground tracks and waveform diversity," in *Proceedings of the IEEE International Geoscience and Remote Sensing Symposium*, pp. 4145–4148, Kuala Lumpur, Malaysia, 2022.

[18] D. Castelletti, G. Farquharson, J. Brown et al., "Capella space VHR SAR constellation: advanced tasking patterns and future capabilities," in *Proceedings of the IEEE International Geoscience and Remote Sensing Symposium*, pp. 4137–4140, Kuala Lumpur, Malaysia, 2022.

[19] M. Huang, Y. Xu, L. Qian et al., "A bridge neural network-based optical-SAR image joint intelligent interpretation framework," *Space: Science & Technology*, vol. 2021, 2021.

[20] J. Zhang, Y. Cai, C. Xue, Z. Xue, and H. Cai, "LEO mega constellations: review of development, impact, surveillance, and governance," *Space: Science & Technology*, vol. 2022, 2022.

[21] M. D'Errico, A. Moccia, and S. Vetrella, "High frequency observation of natural disaster by SAR interferometry," *Photogramm Eng Remote Sensing*, vol. 61, pp. 891–898, 1995.

[22] M. D'Errico and M. D. Graziano, "Analysis of COSMO/Sky-Med application to maritime surveillance of Mediterranean Basin," *Journal of Aerospace Science, Technology & Systems*, vol. 89, pp. 100–110, 2012.

[23] "Mare Mostrum," 2019, (Accessed on 29/08/2023), http://www.legambiente.it/wp-content/uploads/Dossier-Mare-Monstrum-2019.pdf.

[24] "EU action to combat illegal fishing control systems in place but weakened by uneven checks and sanctions by member states," (Accessed on 29/08/2023), http://www.eca.europa.eu/Lists/ECADocuments/SR22_20/SR_Illegal_fishing_EN.pdf.

[25] "AMP," (Accessed: 29/08/2023), http://www.minambiente.it/pagina/aree-marine-istituite.

[26] "Insider," (Accessed on 29/08/2023), http://it.insideover.com/societa/traffico-droga-italia-sicurezza-porti.html.

[27] "Frontex," (Accessed on 16/02/023), http://etendering.ted.europa.eu/document/document-file-download.html?docFileId=36926.

[28] "COSMO-SkyMed Seconda Generazione: system and products description. Doc. No. CE UOT-2021-002, rev. A," 2021.

[29] "COSMO-SkyMed (Constellation of 4 SAR Satellites)," (Accessed on 13/02/ 2023), http://directory.eoportal.org/web/eoportal/satellite-missions/c-missions/cosmo-skymed.

[30] "COSMO-SkyMed second generation (CSG) constellation," (Accessed on 13/02/2023), http://directory.eoportal.org/web/eoportal/satellite-missions/c-missions/cosmo-skymed-second-generation.

[31] "SAOCOM (SAR observation & communications satellite) constellation," (Accessed on 13/02/2023), http://directory.eoportal.org/web/eoportal/satellite-missions/s/saocom.

[32] Recchia, *SAOCOM 1A Quality Assessment Summary. Document EDAP.REP.019, Issue 1.1*, ESA (European Space Agency), 2020.

[33] SIASGE(Accessed on 13/02/2023), http://www.argentina.gob.ar/ciencia/conae/misiones-espaciales/siasge.

[34] "Copernicus: Sentinel-1 — the SAR imaging constellation for land and ocean services," (Accessed on 13/02/2023), http://directory.eoportal.org/web/eoportal/satellite-missions/c-missions/copernicus-sentinel-1.

[35] D. Geudtner, P. Prats, N. Yague-Martinz et al., "Sentinel-1 constellation-SAR interferometry performance verification," in *41st Plenary of the Working Group on Calibration & Validation of CEOS Earth Observation Working Group*, pp. 1–15, Tokyo, Japan, 2016.

[36] M. D. Graziano, M. D'Errico, and E. Razzano, "Constellation analysis of an integrated AIS/remote sensing spaceborne system for ship detection," *Advances in Space Research*, vol. 50, no. 3, pp. 351–362, 2012.

[37] Y. Kozai, "The motion of a close earth satellite," *The Astronomical Journal*, vol. 64, pp. 367–377, 1959.

[38] D. R. Brooks, *An Introduction to Orbit Dynamics and Its Application to Satellite-Based Earth Monitoring Mission*, NASA, Washington, DC, USA, 1977.

[39] K. J. Duck and J. C. King, "Orbital mechanics for remote sensing," in *Manual of Remote Sensing*, R. N. Colwell, Ed., pp. 699–706, American Society of Photogrammetry, Falls Church, VA, USA, 2nd edition, 1983.

[40] J. C. King, "Quantization and symmetry in periodic coverage patterns with applications to earth observation," *The Journal of Astronautical Sciences*, vol. 24, pp. 347–363, 1976.